

FLUID CRACKING CATALYST WITH CARBON SELECTIVITY

M. L. Occelli* and D. C. Kowalczyk
Gulf Research & Development Company
P. O. Drawer 2038
Pittsburgh, PA 15230

ABSTRACT

A fluid cracking catalyst was formed by spray drying a silica sol slurry containing an acid-leached kaolin mineral (with a $\text{SiO}_2/\text{Al}_2\text{O}_3$ ratio of 2.6) and calcined rare earth exchanged zeolite Y (CREY). Microactivity testing (MAT) data show the catalyst (with ~22% CREY) can give 66 vol% conversion in the presence of 5000 ppm Ni-Equivalents. Carbon generation (4.3%) seems to be independent of metals concentration over the range investigated. In the presence of 1.0% vanadium, the catalyst is as active as when metal-loaded with 5000 ppm Ni-Equivalents. With 2% vanadium, there is a drastic decrease in activity. Commercial catalysts have similar activity and gasoline selectivity but generate considerably more hydrogen and carbon, especially at high metals loading.

INTRODUCTION

Oil shortages have, at the present, disappeared, but refiners are nonetheless under economic pressure to process cheaper, metals-contaminated crudes. In fact, because of nationwide conservation efforts, gasoline consumption in the U.S. has and is projected to steadily decline in the 80's. Therefore, refiners without the capability of converting less costly, heavier oils into transportation liquids will suffer competitively in this shrinking energy market (4-6). Several units have already reported using heavy crudes in their FCC operations (7-9).

Catalyst requirements to process Ni- and V-contaminated feedstocks have been described elsewhere; (9-11) a recent discussion has been given by Magee (6). Vanadium is known to destroy catalyst activity, and its effects can be mitigated by tin addition (12). Nickel, while not causing zeolite destruction, generates large amounts of gases and coke, placing severe demands on gas compressors' capability. Antimony organics have been shown to reduce by 50% gas formation due to metal contaminants, especially nickel (13-15). Cracking catalysts capable of forming inactive metal silicates or even aluminosilicates on their surface could crack heavy oils to useful products and minimize coke, hydrogen, and light gas generation.

Examples of silica-bound zeolite containing FCC have been described by Elliot (16), Ostermaier and Elliot (17), Flaherty et al. (18), and Seese et al. (19). It is the purpose of this paper to report a silica-rich cracking catalyst resistant to deactivation by metals contaminants like nickel and vanadium.

*To whom all correspondence should be addressed.

EXPERIMENTAL

Catalyst Preparation

A silica sol was prepared by simultaneously mixing diluted sodium silicate, alum, and sulphuric acid in a manner to keep the slurry pH between 2.8 and 3.2. The sol was then vigorously homogenized and aged for three hours at room temperature. Calcined and acid-washed kaolin ($\text{SiO}_2/\text{Al}_2\text{O}_3=2.6$) was then added to form a slurry containing 639 g SiO_2 , 231.6 g Al_2O_3 , and 126 g clay. Calcined rare earth exchanged zeolite Y (CREY from Davison) was then added to obtain the desired cracking activity. The catalyst zeolite level (% CREY) is defined as $\text{CREY}/(\text{SiO}_2 + \text{Al}_2\text{O}_3 + \text{CLAY} + \text{CREY}) \cdot 100$.

The fluidized cracking catalyst was obtained by spray drying the slurry at ~15-20% solids. The microspheres were slurried in a 5 l 2% NH_4OH solution to remove sodium ions. After a final washing with a large excess of deionized water and drying at 400°C for 10 h, the catalysts were submitted for evaluation. The microspheres with ~22% CREY had 250 m^2/g BET surface area, 0.23 cc/g pore volume, and an average pore radius of 18.6 Å; their bulk density was 0.66 g/cc .

Catalyst Testing

Catalytic evaluation was performed using a microactivity test similar to the one described by Ciappetta and Henderson (1). The weight hourly space velocity was 15 with 80 sec catalyst contact time at $T = 480^\circ\text{C}$. The charge stock was a Kuwait gas oil having a 260°-426°C boiling range (see Table 1); a catalyst-to-oil ratio of 2.5 was used. Prior to testing, catalysts were steam-aged for 10 h at 730°C with a ~50-50% N_2 -steam mixture. (Ni-V) naphthenates were used to metal-load fresh catalysts according to a procedure described elsewhere (2). Ni-equivalents is defined as the sum $(\text{Ni} + 1/5 \text{V})$ expressed in parts per million (ppm). Percent conversion is defined as: $(V_f - V_p) 100/V_f$ where V_f is the volume of the fresh feed (FF) and V_p is the volume of product boiling above 204°C.

RESULTS AND DISCUSSION

As expected (3), cracking activity of this silica-rich catalyst increases with zeolite content (Figure 1). In the 15-22% CREY range, conversion changed from 74 to 81.6%. Gasoline make remained at ~53%; this and the increase in hydrogen and carbon generation indicates the occurrence of overcracking, Figures 2, 3, and 4.

Metals (Ni + 1/5 V) effects on catalyst activity are given in Figures 5-8. Losses in gasoline yields follow the decrease in catalyst activity with metal loadings (Figures 5 and 6) since both effects are due to losses in catalyst crystallinity. The silica-rich catalyst (with 15 or 22% CREY) deactivates in a manner similar to that of a commercial catalyst having comparable initial activity (Figure 5). The catalyst (with ~22% CREY) appears to be more selective with respect to hydrogen generation (Figure 7), and its carbon make (~4.3%) is independent of metals loading up to 5000 Ni-Equivalents. In contrast, the commercial catalyst carbon generation monotonically increases with metals level (Figure 8). Both catalysts have similar resistance to vanadium poisoning. In the presence of 1.0% V conversion was ~60% (down from ~82% for the fresh catalysts); with 2% V, cracking activity was reduced to ~30%. The silica-rich matrix of the catalyst did not prevent zeolite destruction by the vanadium. CREY has a strong diffraction peak at $2\theta=23.8^\circ$. With 1% V, the original peak intensity was reduced by ~50%; with 2% V, evidence of crystallinity disappeared.

Results in Table 2 show the silica-rich catalyst's hydrothermal stability (50/50% nitrogen-steam for 10 h at 730°C) and carbon selectivity. Even after steaming at 815°C for 5 h with 95% steam the catalyst was able to retain 90% of the cracking activity measured after aging with 50% steam. Steaming, however, affects the stability of vanadium-contaminated catalysts. In fact, after aging with 95% steam (10 h at 730°C) microspheres with 0.5% V retained ~70% of their initial activity; with 0.75% V, they became inactive. X-ray diffractograms showing crystallinity losses due to vanadium loadings are given in Figure 9.

Without metals, the steam-aged catalyst had 177.8 m²/g BET surface area, 0.19 cc/g nitrogen pore volume, and an average pore radius of 21.2 Å. In Figure 10 its carbon selectivity is represented as the weight of carbon by-product per volume percentage of conversion. This value is plotted as a function of conversion to show that for conversion levels in the 65 to 80% range, the silica-rich catalyst generates lower coke yields than the commercial cracking catalysts tested.

The use of acid-leached calcined kaolin has little effect on a fresh catalyst (with ~15% CREY) activity, but it may increase gasoline yields, see Table 3. The catalyst exhibits improved resistance to metals deactivation when it contains an acid-leached calcined kaolin mineral (with SiO₂/Al₂O₃ = 2.6) instead of untreated kaolin. The acid treatment removes aluminum and establishes octahedral vacancies in the mineral lattice. These "holes" could host metals like Ni and V and negate their deleterious effects on cracking activity and product selectivities. The catalyst's low carbon generation has probably been enhanced by its silica-rich matrix's ability to form inert nickel silicates. Nickel passivation, due to silicates formation, has been previously postulated by Meisenheimer (20) for amorphous (silica-alumina) cracking catalysts.

REFERENCES

1. F. Ciapetta and D. Henderson, *Oil and Gas Journal*, 65, 88 (1967).
2. B. R. Mitchell, *Ind. Eng. Chem. Prod. Res. Dev.*, 19, 209 (1980).
3. J. S. Magee and J. J. Blazek, "Zeolite Chemistry and Catalysis," ACS Monograph #171, J. A. Rabo, Ed., 615 (1976).
4. C. P. Reeg, NPRA Annual Meeting, AS82-3, 1 (1982).
5. C. P. Carter, *Hydro. Proc.*, 96 (1981).
6. J. S. Magee, "Adv. in Cat. Chem., II Symposium," Salt Lake City, Utah (1982).
7. J. R. Murphy and A. K. Logwinuk, NPRA Annual Meeting, AMS1-29, 11 (1981).
8. R. E. Ritter et al., NPRA Annual Meeting, AM81-44, 1-4 (1981).
9. R. E. Ritter et al., *Oil and Gas Journal*, 103 (1981).
10. R. N. Cimbalò et al., *Oil and Gas Journal*, 112 (1972).
11. J. G. Sikonia et al., *Oil and Gas Journal*, 141 (1981).
12. A. English and D. C. Kowalczyk, *Oil and Gas Journal* (1984), to be submitted.
13. J. R. Murphy in "Sym. Prod., Character., Process of Heavy Oils, etc.," University of Utah, 5 (1981).

14. J. W. Gall et al., NPRA Annual Meeting, AM82-50, 5 (1982).
15. D. L. McKay and B. J. Bertus, "Symp. on Advances in Petr. Proc.," Div. of Petr. Chemistry Preprints 24, 2, 645 (1979).
16. C. H. Elliot, Jr., U.S. Patent No. 3,867,308 (1975).
17. J. J. Ostermaier and C. H. Elliot, Jr., U.S. Patent No. 3,957,689 (1976).
18. T. V. Flaherty, Jr., et al., U.S. Patent No. 4,126,579 (1978).
19. M. A. Seese et al., U.S. Patent No. 4,226,743 (1980).
20. R. G. Meisenheimer, J. Cat., 1, 356 (1962).

WPC#4082

Table 1. Kuwait gas oil inspections.

Gravity, API	23.5
Viscosity, 130°F	94.7
Viscosity, 150°F	70.5
Viscosity, 210°F	50.8
Pour Point, °F	+80
Nitrogen, wt%	0.074
Sulfur, wt%	2.76
Carbon, Res., wt%	0.23
Bromine No.	5.71
Aniline Point, °F	176.5
Nickel, ppm	<0.1
Vanadium, ppm	<0.1
Distillation, at 760 mm	
End Point, °C	426
5 Pct. Cond.	263
Approx. Hydrocarbon Type Analysis: vol%	
Carbon as Aromatics	23.1
Carbon as Naphthenes	10.5
Carbon as Paraffins	66.3

Table 2. Hydrothermal stability data of a SiO₂-rich cracking catalyst containing ~22% CREY. Steaming was performed with a 50-50% steam-nitrogen mixtures at 1 atm for 10 h.

	<u>Steaming Temperature (°C)</u>		
	<u>730</u>	<u>760</u>	<u>790</u>
Conversion (V%ff)	81.26	80.06	76.03
Gasoline (V%ff)	52.83	54.92	52.45
Hydrogen (wt%ff)	0.03	0.02	0.02
Carbon (wt%ff)	3.99	3.56	3.20

Table 3. Effects of an acid-leached kaolin mineral on the metals resistance of a FCC containing ~15% CREY. Test conditions: T = 480°C, Kuwait G0; aging with 50% steam for 10 h at 730°C.

Kaolin (SiO ₂ /Al ₂ O ₃)	2.6	2.6	2.0	2.0
Metals (Ni-Equiv.)	0	3000	0.0	3000
Conversion (V%ff)	72.2	62.9	72.9	51.0
Gasoline (V%ff)	52.1	42.5	50.2	32.9
Hydrogen (wt%ff)	0.05	0.50	0.03	0.44
Carbon (wt%ff)	2.78	2.94	2.46	3.04

Figure 1 Cracking Activity

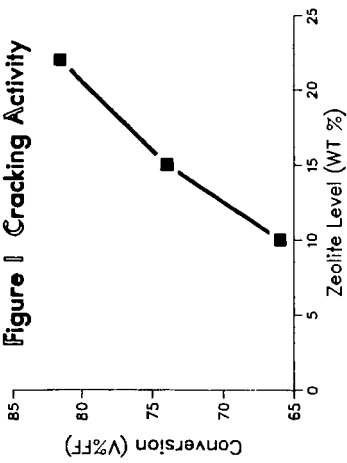


Figure 3 Hydrogen Yields

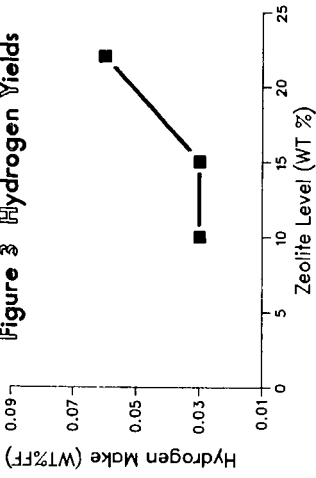


Figure 2 Gasoline Yields

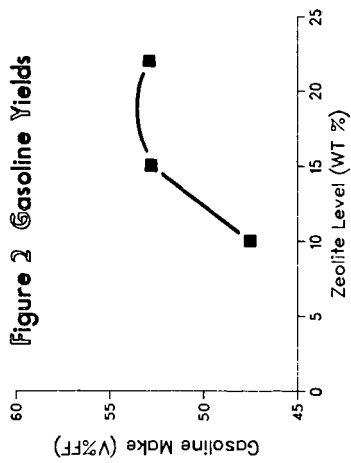


Figure 4 Carbon Yields

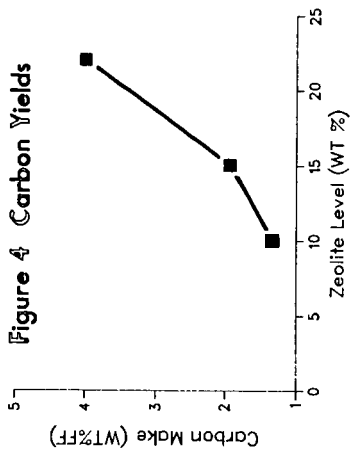


Figure 5 Metal (Ni + V) Effects on Catalyst Activity

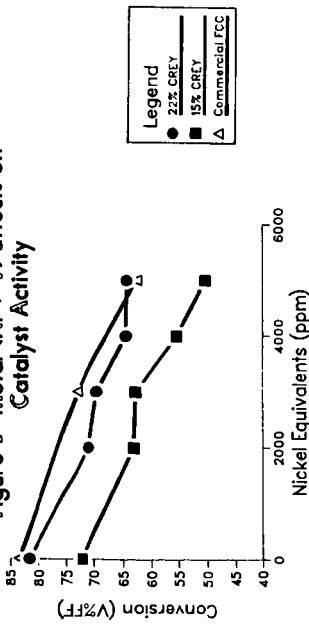


Figure 7 Metal (Ni + V) Effects on Hydrogen Make

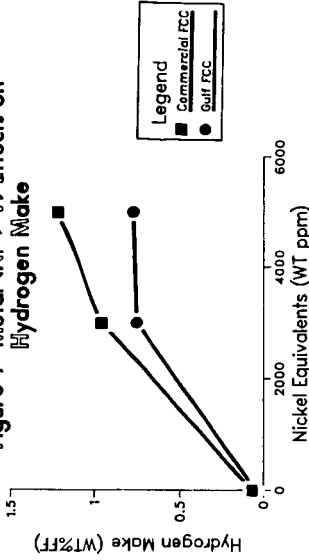


Figure 6 Metal (Ni + V) Effects on Gasoline Generation

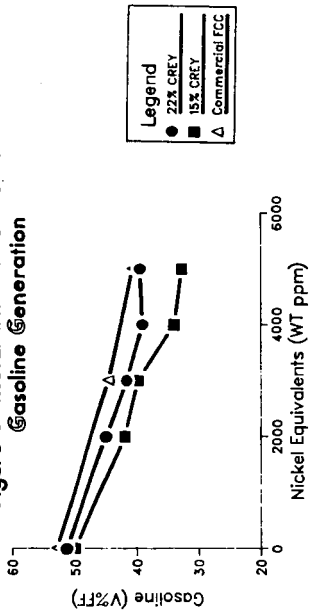


Figure 8 Metal (Ni + V) Effects on Carbon Make

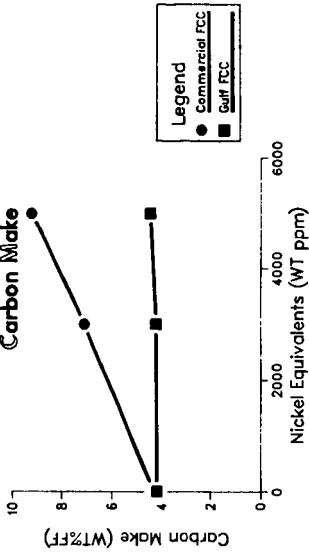


FIGURE 9:

X-RAY DIFFRACTOGRAMS SHOWING VANADIUM EFFECTS ON CRYSTALLINITY. CATALYSTS WERE STEAMED FOR 10h AT 730°C, WITH 95% STEAM AT 1atm.

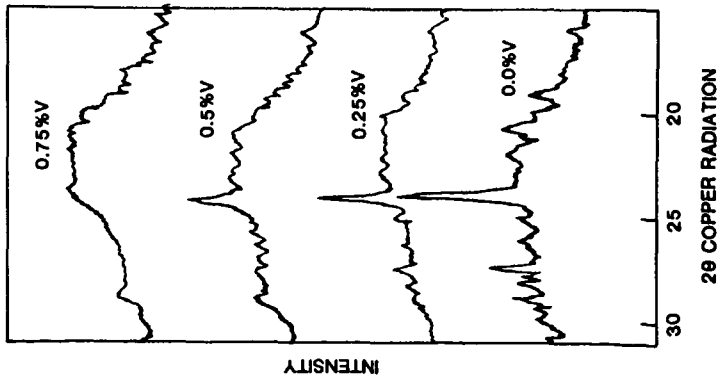
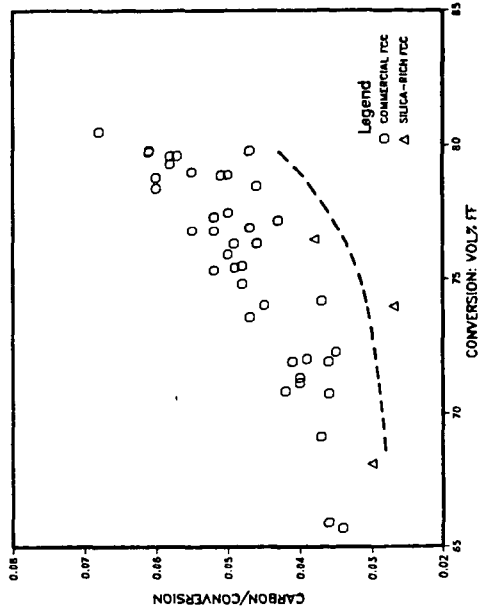


FIGURE 10
GULF SILICA-RICH FCC CATALYST
MAT CARBON SELECTIVITY



HYDROCRACKING WITH PILLARED CLAYS

Mario L. Occelli* and Raymond J. Rennard
Gulf Research & Development Company
P.O. Drawer 2038
Pittsburgh, PA 15230

ABSTRACT

Pillared bentonites have been prepared by ion-exchanging the clay charge compensating cations with zirconyl-aluminum halohydroxy complexes $(ZrOCl_2 \cdot Al_8(OH)_{20})^{+4}$, hydroxyaluminum oligomers $[Al_{13}O_4(OH)_{24}(H_2O)_{12}]^{+7}$ and colloidal silica. These interlayered clays have 250-320 m^2/g BET surface area, 0.15-0.22 cc/g pore volume, and pore height between 6 and 9 Å; thermal stability (in air, 10 h) is limited to 550°C. After a mild thermal pretreatment at 400°C in air, their cracking activity for gas oil conversion was related to the clay cations in the following manner: $Ca \ll (Si, Al) < (Zr, Al) < Al$.

Pillared clays were evaluated for use both as a cracking component and a hydrogenation component (Ni and Mo) support for the hydrocracking of an Agha Jari vacuum gas oil (VGO) in a combined hydrodenitrogenation-hydrocracking (HDN-HC) upgrading reactor. When used as the hydrocracking component with an Al_2O_3 hydrogenation support, catalyst activity was: Ca-bentonite < (Al,Zr)-bentonite < ACH-bentonite < HY zeolite. When used as the hydrogenation component support with 30 wt% HY zeolite as the cracking component, the activity order was $Al_2O_3 \ll (Al,Zr)$ -Bentonite < (Si-Al)-Bentonite < ACH-bentonite. Pillared bentonites based hydrotreating catalysts showed superior selectivity to middle distillates.

INTRODUCTION

Bentonites pillared with oxoaluminum cations are characterized by an open, two-dimensional pore structure which behaves like a strong Lewis acid and allows sorption and transport of branched aromatics and normal paraffins.⁽¹⁻³⁾ Mesitylene diffusion in a pillared Na-bentonite is twice as fast as in Na-Y zeolite⁽⁴⁾ and is characterized by an apparent energy of activation (6.4 kcal/mole) similar to that observed for the transport of 1,3,5-triisopropylcyclohexane in NaY. C_5 - C_{10} normal paraffin equilibrium loadings resemble those observed in Mobils' ZSM-5; diffusion coefficients are, in general, significantly greater than those measured in zeolites.⁽³⁾ Therefore, pillared clays could find utility as catalysts for converting high molecular weight hydrocarbons like those found in heavy oils.^(5,6)

After mild steam deactivation, pillared clays exhibit cracking activity for gas oils conversion comparable to that of commercial cracking catalysts containing 15 to 25% zeolite, but they generate two to three times as much coke in the 60-80% conversion range.^(5,7) Coking experiments have shown that catalytic coke may not be the main cause of catalyst deactivation during gas oil conversion. Coking

* To whom all correspondence should be addressed.

has been attributed primarily to hydrocarbon occlusion and thermal degradation within the pillared clay microspace.⁽⁸⁾

The following paper reports the effects of using pillared clays as cracking components or as a metals support component in composite hydrogenation-hydrocracking vacuum gas oil catalysts.

EXPERIMENTAL

Pillared Clays Preparation

Pillared clays were prepared with a bentonite sample obtained from the American Colloid Company; its chemical composition is shown in Table 1. The aluminum chloro-hydroxide (ACH) solution containing the $(Al_{13}O_4(OH)_{24}(HO)_{12})^{+7}$ cation and the solution containing the $(Al_8(OH)_{20}ZrO)^{+6}$ complex (RETZEL-36G) were obtained from the Reheis Chemical Company. Colloidal silica, with a SiO_2/Al_2O_3 ratio of 16, was provided by NALCO Chemicals. These solutions were added to a 20-L slurry containing 100 g of bentonite. After stirring the slurry for 1-2 h at 65°C the clay was filtered and then reslurried in 5 L of distilled water (at 65°C) to remove excess reactants. After a second filtration and wash, the clay was dried at 120°C, crushed, and sized to <100 mesh and then used for hydrotreating catalysts preparation. X-ray diffractograms of these pillared clays are shown in Figure 1; their composition is given in Table 1.

Catalyst Forming

Two forming methods were employed. When the clay was used as the cracking component, a Harshaw Al-4100P alumina hydrate powder was calcined at 400°C and then loaded with 4% Ni-14% Mo via a one-step, co-impregnation with nickel nitrate-ammonium paramolybdate solution. The oven-dried impregnated alumina was then mix-mulled with the clay, peptized with 1% nitric acid, and extruded. The extrudates were oven-dried overnight at 120°C and then calcined at 450°C for 18 h. The composition of the finished catalysts were by weight, 70% (4 Ni-14 Mo/ Al_2O_3) + 30% clay.

When clays were used as metals support, the pillared bentonite was calcined at 400°C and then loaded with 4 Ni-14% Mo by weight using the same one-step procedure described above. The oven-dried, metals-loaded clay was then mix-mulled with ammonium Y zeolite, peptized with 1% nitric acid, and extruded. The extrudates were heat-treated as before; their composition (in wt%) were 70% (4 Ni-14 Mo/clay) + 30% HY. The ammonium Y zeolite was prepared by NH_4^+ -exchanging Linde NaY until the residual sodium level was less than 0.5%.

Catalyst Testing

Pillared bentonite cracking activity was evaluated by a microactivity test similar to the one described by Ciapetta and Anderson.⁽⁹⁾ Test conditions as well as chargestock inspections are described elsewhere.⁽⁷⁾ Before testing, catalysts were heated (in dry air) at 400°C for 10 h. Percent conversion is defined as: $(V_f - V_p) / 100 V_f$ where V_f is the volume of the fresh feed (FF) and V_p is the volume of product boiling above 204°C.

HDN-HC runs were conducted in an externally heated 1.43 cm ID by 122 cm stainless steel, down flow, trickle bed reactor. A 0.48 cm OD concentric thermowell running the length of the reactor was used to monitor temperatures in the reactor zones. For all runs a 75 mL catalyst bed was employed. The top 35 mL of catalyst was a commercially available Nalco NM-504 hydrotreating catalyst. The bottom 35 mL of the bed was loaded with the experimental composite hydrocracking catalyst to be evaluated. No product separation was carried out between catalyst beds. Both catalysts were sized to 16x40 mesh and presulfided in situ at 204°C and 35 psig for 6 h with 56 L/h of a 92% hydrogen-8% hydrogen sulfide gas blend.

An Agha Jari VGO containing 1500 ppm organic nitrogen and 1.2% sulfur was the feed for all runs. The reaction conditions in Table 2 were chosen to allow the hydrotreating catalyst to reduce the feed organic nitrogen and sulfur levels to <50 ppm and <0.2%, respectively; reactor configuration is shown in Figure 2. Hydrocracking test runs were 34 h in duration, with a 2-h off-stream period and five, 3 h on-stream periods at each temperature. Analyses were performed on products collected from the last on-stream period.

RESULTS AND DISCUSSION

Exchange reactions of Ca-bentonite with polynuclear cations generate molecular sieve-like materials stable to 500-600°C with 250-320 m²/g surface area and 0.15-0.22 cc/g pore volume (Tables 1 and 3). This microspace is attributed to the pillaring induced by stable oxide clusters formed by dehydroxylating the inter-layering cations. As in HY zeolites, pillared clays exhibit a narrow distribution of pore sizes with more than 85% of this area in pores with radius less than 10 Å, Table 3. At cracking conditions (400°C) in vacuo acidity in clays pillared with aluminum oxide clusters is mostly of the Lewis type; a Lewis/Bronsted (L/B) acid sites ratio of four has been found.⁽⁶⁾ In HY, a L/B ratio of 0.6 has been estimated from literature data.⁽⁶⁾ In powder form (100 x 325 mesh granules) pillared bentonites have (after aging in air at 400°C/10 h) cracking activity for gas oil conversion similar to that of HY (Table 4). The ranking is as follows:

Ca-Bentonite << (Si,Al)Bentonite < (Zr,Al)Bentonite < ACH-Bentonite < HY

However, the HY zeolite retains useful cracking activity even after a hydrothermal (10 h at 730°C with 95% steam at 1 atm) aging period, whereas pillared clays do not.

To isolate the two catalysts contribution to the overall HDN-HC activity, blank runs were performed with the composite catalyst bed replaced with 37.5 mL of inert, fired quartz chips. Results in Table 5 show the ability of the commercial hydrotreating catalyst (Nalco NM-504) for sulfur and nitrogen removal. The decrease of the 360°C⁺ fraction with temperature indicate its activity for hydrocarbon cracking; therefore, conversion over the combined HDN-HC catalyst at each temperature is expressed as,

$$CON = 100 \times (TGO^B - TGO^R) / TGO^B,$$

where TGO^B and TGO^R are the 360°C⁺ content of the blank and run product, respectively.

Three clays (Ca-bentonite, ACH-bentonite, and (Al,Zr) bentonite) were tested, along with HY, as cracking components in composite catalysts containing 70% alumina loaded with 14% Mo and 4% Ni. Results in Table 6 show that bentonite pillared with Al_2O_3 -clusters (ACH-bentonite) is the most active clay for VGO cracking; at 400°C it is significantly less active than the HY-containing catalyst. While the relative ranking of the catalysts in terms of activity is the same as that observed in cracking gas oils, the hydrocracking activity differences between pillared clays and HY zeolite are much more pronounced. At 415°C this difference is even more evident (see Table 6). In fact, while the activity of the zeolite-containing catalyst increases to 98.3% (up from 48.2% at 400°C), the activity of the ACH-bentonite containing catalyst remained unchanged at 31-32%. Rapid deactivation due to hydrocarbons occlusion and coking, is believed responsible for the pillared clays apparent low hydrocracking activity (see Table 6).

ACH-bentonite (Si,Al)-Bentonite and (Al,Zr)-Bentonite were used as metal (14% Mo + 4% Ni) support in composite catalysts promoted with 30% HY for hydrocracking activity. A similar catalyst containing metal-loaded alumina (and 30% HY) was used as reference material. Results in Table 7 indicate the greater activity of the pillared clays containing catalysts and their selectivity with respect to light furnace oil (LFO) generation. The rapid deactivation previously observed was not evident in these runs. Metal loading the pillared clays may have reduced their acidity and minimized coke formation. (Al,Zr) pillared bentonite has greater cracking activity than (Si,Al) bentonite (Table 4). The higher hydrocracking activity of the (Si,Al) bentonite composite catalyst with respect to the one containing (Zr,Al) Bentonite (see Table 7) is due to the different surface area of these pillared clays (Table 3). As expected, the ACH-bentonite containing catalyst was most active. At 400°C conversion was 70% and generated a liquid containing 37.7% LFO. The selectivity of these clays for LFO production during VGO hydrocracking can be attributed to the pillared clay microporous structure, which appears to control the cleavage of high molecular weight hydrocarbons and retards further cracking to lighter fractions.

CONCLUSION

Because of rapid deactivation due to excessive coke formation, pillared clays are ineffective when used as the cracking component in composite hydrocracking catalysts. When used as metals supports in composite catalysts containing zeolites, the pillared clays show excellent hydrocracking activity and selectivity to light furnace oil. This is probably due to the moderation of their acidity resulting from the addition of hydrogenation metals like Mo and Ni and to the open microstructure resulting from pillaring.

REFERENCES

1. D. E. W. Vaughan and R. J. Lussier, "Preparation of Molecular Sieves Based on Pillared Interlayered Clays (PILC)," Proc. 5th Inter. Conf. Zeolites," L. V. Rees, Ed., Heyden, London 1980, 94.
2. M. L. Occelli, and R. M. Tindwa, "Physicochemical Properties of Montmorillonite Interlayered with Cationic Oxyaluminum Pillars," Clays and Clay Minerals 1983, 31, 1, 22.

3. M. L. Occelli, V. Parulekar, and J. W. Hightower, Proc. 8th Inter. Congress Catalysis, Berlin (1984), in press.
4. M. L. Occelli, R. A. Innes, F. S. S. Hwu, and J. W. Hightower, "Catalytic Activity of Sodium-Montmorillonite Interlayered with Aluminum Oxide Clusters," J. Applied Catalysis 1984, Submitted.
5. D. E. W. Vaughan, R. J. Lussier, and J. S. Magee (1970), U.S. Patent No. 4, 175,090.
6. D. E. W. Vaughan, R. J. Lussier, and J. S. Magee (1981), U.S. Patent No. 4, 248,739.
7. M. L. Occelli, I&EC Prod. Res. Dev. Journal 1983, 22, 4 (1983), p. 553.
8. M. L. Occelli and J. E. Lester, I&EC Prod. Res. Dev. Journal (1984), Submitted.
9. F. G. Ciapetta and D. Anderson, Oil and Gas J., 65 (1967), 88.

FIGURE 1:

X-RAY DIFFRACTOGRAMS OF (a) BENTONITE BEFORE AND AFTER PILLARING WITH (b) Al (c) Al AND Zr (d) Al AND Si OXIDE CLUSTERS. CLAYS WERE HEATED FOR 10H AT 300°C IN AIR

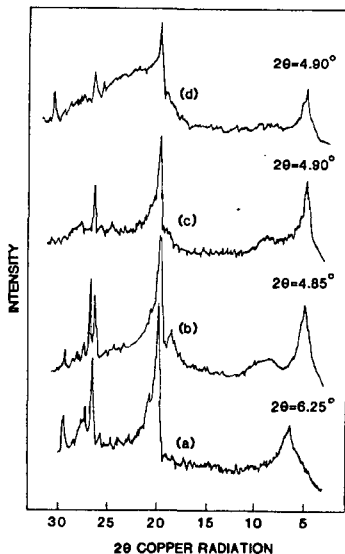


Figure 2

HDN-HC REACTOR CONFIGURATION

o
T C = 380-415
LHSV = 1.0
PSIG = 2000
H₂, scf/bbl = 6000
2
FEED = AGHA JARI VGD
S, wt% = 1.75
N, ppm = 1500
o
API = 23.1

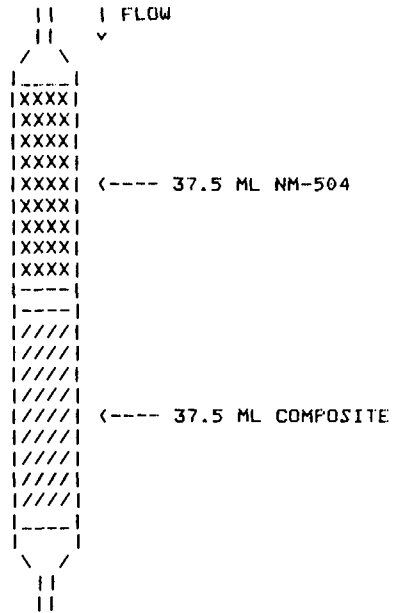


Table 1. Bentonite composition before and after pillaring (Galbraith Laboratories Data).

	Oxides Composition (Wt%)			
	Calcium Bentonite	ACH- Bentonite	(Zr-Al) Bentonite	(Si-Al) Bentonite
SiO ₂	62.9	55.9	55.3	78.1
Al ₂ O ₃	20.0	31.6	25.8	13.9
Na ₂ O	0.53	0.67	0.50	0.35
K ₂ O	2.32	0.37	0.35	0.20
MgO	2.16	1.55	1.58	0.90
CaO	2.58	0.43	0.24	0.48
Fe ₂ O ₃	4.38	3.59	3.60	1.8
ZrO ₂	--	-	6.1	--

Table 2. Hydrotreating-hydrocracking run conditions.

Feedstock	Agha Jari V60
Gravity, °API	23.1
Sulfur, wt%	1.75
Nitrogen, ppm	1500
Temperature, °C	390-415
Pressure, kpa (psig)	13,891 (2000)
Catalyst Volume, mL	37.5 Hydrotreating 37.5 Hydrocracking
Catalyst Bed Length, cm	52.8
LHVS, h ⁻¹	1.0
Feed Volume, mL/h	75
Hydrogen/Oil, m ³ /m ³ (scf/bbl)	1069 (6000)

Table 3. Pillared clays surface properties after heating in dry air at 400°C/10 h and sizing to 100x325 mesh granules.

	<u>ACH-</u> <u>Bentonite</u>	<u>(Zr,Al)</u> <u>Bentonite</u>	<u>(Si,Al)</u> <u>Bentonite</u>	<u>Calcium</u> <u>Bentonite</u>	<u>HY</u> <u>Linde</u>
BET Surface Area (m ² /g)	255.0	254.0	303.5	46.6	508
Pore volume (cc/g)	0.16	0.17	0.21	0.08	0.32
Pore Volume Distribution					
Area % in Pores with Radius					
< 10 Å	88.0	90.0	87.8	25.2	94.9
10 < R < 20 Å	9.4	7.1	8.6	36.1	2.3
20 < R < 100 Å	2.4	2.4	3.2	29.1	1.4
> 100 Å	0.2	0.5	0.4	9.6	1.4

Table 4. Cracking activity for gas oil conversion before and after pillaring. Clays were heated at 400°C/10 h in dry air and sized to 100 x 325 mesh before testing.

	<u>Calcium</u> <u>Bentonite</u>	<u>ACH-</u> <u>Bentonite</u>	<u>(Zr,Al)</u> <u>Bentonite</u>	<u>(Si,Al)</u> <u>Bentonite</u>
Conversion (V% ff)	28.4	82.1	73.8	67.9
Gasoline (V% ff)	16.7	59.8	55.6	51.5
Furnace Oil (V% ff)	30.3	13.6	19.0	22.3
Slurry Oil (V% ff)	41.6	4.2	7.2	9.8
Hydrogen (wt% ff)	0.75	0.24	0.21	0.28
Carbon (wt% ff)	7.8	12.2	9.6	7.48

Table 5. HDN-HC blank runs.

<u>Component</u>	<u>T°C</u>	<u>% NAP</u>	<u>% KER</u>	<u>% LFO</u>	<u>% TGO</u>	<u>°API</u>	<u>% CON</u>	<u>% S</u>	<u>ppm N</u>
Quartz	380	0.9	3.5	15.6	83.4	28.3	0	0.0	50
Quartz	390	1.6	3.9	16.9	81.5	32.3	0	0.0	30
Quartz	400	3.3	7.8	24.1	72.6	31.2	0	0.0	<20
Quartz	415	6.6	13.5	32.2	61.2	33.3	0	0.0	<10

Table 6. HDC-HC with pillared clays as cracking component.

<u>Cracking Component</u>	<u>Reactor</u>		<u>Liquid Composition*</u>				
	<u>T°C</u>	<u>% NAP</u>	<u>% KER</u>	<u>% LFO</u>	<u>% TGO</u>	<u>°API</u>	<u>% CON</u>
HY Zeolite	400	28.0	29.5	34.4	37.6	41.3	48.2
	415	80.0	34.1	18.1	1.0	54.1	98.3
ACH-Bentonite	400	11.6	21.9	39.0	49.5	36.5	31.8
	415	14.2	26.8	43.9	41.9	37.9	31.5
(Al,Zr) Bentonite	400	9.2	14.9	31.2	59.7	34.6	17.8
	415	11.8	19.0	36.6	51.7	36.2	15.5
Ca-Bentonite	400	6.6	14.3	32.7	60.6	34.4	16.5
	415	11.6	21.7	41.4	47.0	36.6	23.2

NAP = Naptha (OP-154°C)

LFO = Light Furnace Oil (190-360°C)

KER = Kerosene (190-271°C)

TGO = Total Gas Oil (360°C+)

Table 7. HDN-HC with clays as hydrogenation component support at 400°C.

Support	Reactor T°C	Liquid Composition*					
		% NAP	% KER	% LFO	% TGO	°API	% CON
Alumina	390	13.1	17.5	28.4	58.6	35.4	28.1
	400	28.0	29.5	34.4	37.6	41.3	48.2
(Al,Zr) Bentonite	390	14.6	25.2	34.6	50.8	36.0	37.7
	400	27.2	32.0	36.4	36.4	40.5	49.9
(Si-Al) Bentonite	390	21.4	26.9	36.7	41.9	39.5	48.6
	400	34.5	30.5	35.8	39.6	42.9	59.2
ACH-Bentonite	390	20.3	34.6	43.4	36.3	40.5	55.5
	400	40.6	35.7	37.7	21.7	45.0	70.1

(a) NAP = Naphtha (OP-154°C); (b) KER = Kerosene (190-271°C); (c) LFO = Light Furnace Oil (190-360°C); (d) TGO = Total Gas Oil (360°C+).

Table 8. HDN-HC with clays as hydrogenation component support at 390°C.

Component	T°C	% NAP	% KER	% LFO	% TGO	°API	% CON
Alumina	390	13.1	17.5	28.4	58.6	35.4	28.1
ACH-Bentonite	390	20.3	34.6	43.4	36.3	40.5	55.5
Si-Bentonite	390	21.4	26.9	36.7	41.9	39.5	48.6
Al,Zr-Bentonite	390	14.6	25.2	34.6	50.8	36.5	37.7

(a) NAP = Naphtha (OP-154°C); (b) KER = Kerosene (190-271°C); (c) LFO = Light Furnace Oil (190-360°C); (d) TGO = Total Gas Oil (360°C+).

CATALYTIC HYDROPROCESSING OF ACIDIC FRACTIONS
OF COAL LIQUID HEAVY DISTILLATE

by

D. W. Grandy and L. Petrakis

Gulf Research & Development Company
P.O. Drawer 2038
Pittsburgh, PA 15230

and

Cheng-lie Li and Bruce C. Gates

Department of Chemical Engineering
University of Delaware
Newark, DE 19711

Individual compound and molecular class kinetics were determined for the catalytic hydrodeoxygenation of coal liquid acid fractions. The coal liquid acidic fractions were prepared from a coal liquid heavy distillate, derived from Powhatan #5 coal, by ion exchange chromatography(1). A commercial sulfided Ni-Mo/ γ -Al₂O₃ catalyst was used to hydrotreat the coal liquid acids which were fed through a microreactor as a 0.25 wt% solution in cyclohexane. The coal acid feeds and hydrotreated products were separated by capillary column gas chromatography and detected by either standard FID techniques or by mass spectrometry. Upon hydrotreating, the product chromatograms (Figure 1) show a large increase in the number of compounds relative to the feed (Figure 2) and a shift to lower boiling range. This change in the chromatogram, and the change in carbon number distribution in the product molecules demonstrates that cracking as well as hydrogenation is taking place. Since many of the feed and product compounds could only be identified by their empirical formula, the results of the catalytic hydrotreating of the acidic fractions can be described in terms of carbon number classes and classes which denote the degree of saturation of the compounds. The carbon number data show evidence of cracking, while the Z numbers, which indicate the degree of saturation, show that compounds of the biphenyl class decrease in relative concentration with increased inverse space velocity; and compounds of the tetralin, indane, and cyclohexylbenzene class show an increase in relative concentration with increased inverse space velocity. Tables I and II list the compound classes identified in the feed and hydrodeoxygenated product of the very

weak and weak acids, respectively. The formation of most of the product molecules can be rationalized using the pure compound hydroprocessing data on cyclohexyl phenol; phenyl phenol(2) and naphthol(3). The examination of the feed and products in terms of the lumps illustrates several points: 1. The feeds contain a relatively small number of major components which, upon hydrotreating, are reduced in concentration, forming many more product molecules. 2. In addition to the removal of the oxygen functionality typically occurring as in the hydroxyl group, there was significant ring hydrogenation. 3. There is evidence of cracking, both from the formation of compounds having fewer carbons than the feed compound and from shifts in carbon number distributions among the compounds existing in the feeds; this cracking is inferred to involve principally the methyl substituents bonded to rings(4).

The hydrodeoxygenation kinetics of tetrahydronaphthol, methyl-tetrahydronaphthol, phenylphenol, methylphenylphenol, dimethylindanol, and cyclohexylphenol are shown in Figure 3 in a plot of fraction of species unconverted vs. inverse weight hourly space velocity. Methyl substitution tends to increase the rate of disappearance of the parent compound, probably by providing an additional pathway for the change in molecular structure. Neither this observation, nor the order of reactivity in disappearance implies hydrodeoxygenation reactivity(5). Methyl groups may hinder heteroatom removal, in some cases, if they prevent easy access to the catalyst by steric hindrance.

1. L. Petrakis, R. G. Ruberto, and D. C. Young, Ind. Eng. Chem. Process Des. Dev. 22, 292 (1983).
2. S. Krishnamurthy, S. Panvelker, and Y. T. Shah, AIChE J. 27, 994 (1981).
3. C. L. Li, Z. R. Xu, Z. A. Cao, and B. C. Gates, Submitted for publication.
4. J. F. Patzer II, R. J. Ferrauto, A. A. Montagna, Ind. Eng. Chem. Process Des. Dev. 18, 625 (1979).
5. C. L. Li, S. S. Katti, B. C. Gates, and L. Petrakis, J. Cat. 85, 256 (1984).

Table I

Number of Compounds by Type in the Very Weak Acid
Feed and Hydrotreated Product

<u>Compound Type</u>	<u>Feed</u>	<u>Product^a</u>
Benzene	9	13
1-Ring Phenols	2	NF ^b
2-Ring Phenols	4	NF
Carbonyl Compounds ^c C-	8	NF
Ethers ^d , R-O-R	6	6
Nitrogen Compounds	6	1
3-Ring Aromatics	1	2
Cyclic Alkanes, Alkenes	NF	7
2-Ring Aromatics	NF	5
Fused Cycloalkyl Aromatics ^e	NF	15
Cycloalkyl Aromatics	NF	4

^a Obtained at a space velocity of 0.4 g of fraction/
(g of catalyst·h).

^b Not found.

^c Furanone is considered to be a carbonyl compound.

^d Ethers include methoxy, phenoxy, and furan.

^e Fused cycloalkyl aromatics include tetralin and indanes.

Table II

Number of Compounds by Type in the Weak Acid Feed
and Hydrotreated Product

<u>Compound Type</u>	<u>Feed</u>	<u>Product^a</u>
Benzenes	4	3
2-Ring Phenols	8	3
Carbonyl Compounds	1	NF ^b
Ethers	2	3
Nitrogen Compounds	2	NF
Cyclo- and Dicycloalkanes, Alkenes	NF	9
Fused Cycloalkylaromatics	NF	14
2-Ring Aromatics or ???	NF	5
3-Ring Aromatics	NF	3
Cycloalkylbenzenes	NF	3

^a Obtained at a space velocity of 0.78 g of fraction/
(g of catalyst·h).

^b Not found.

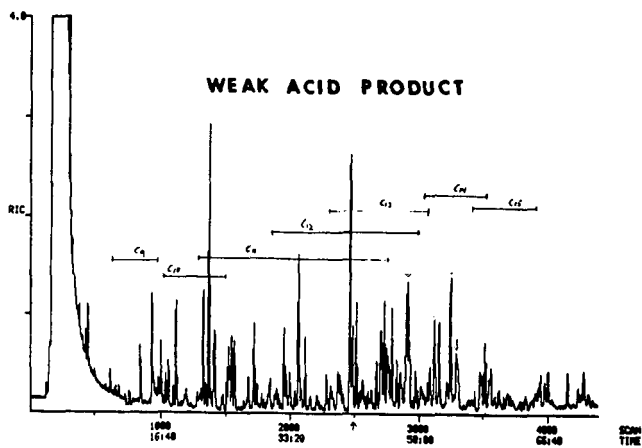


Figure 1

Weak Acid Product Ion Chromatogram

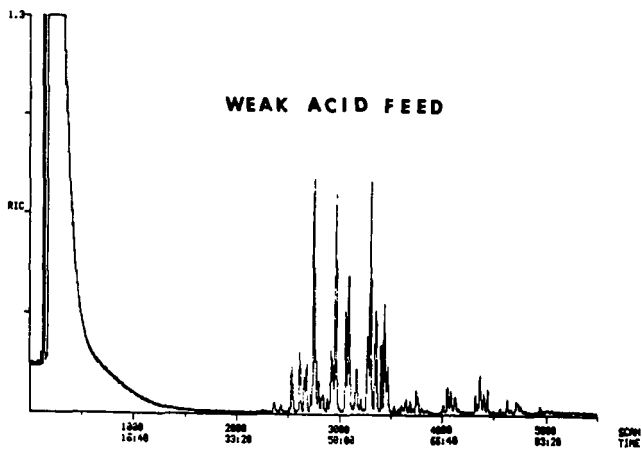


Figure 2

Weak Acid Feed Ion Chromatogram

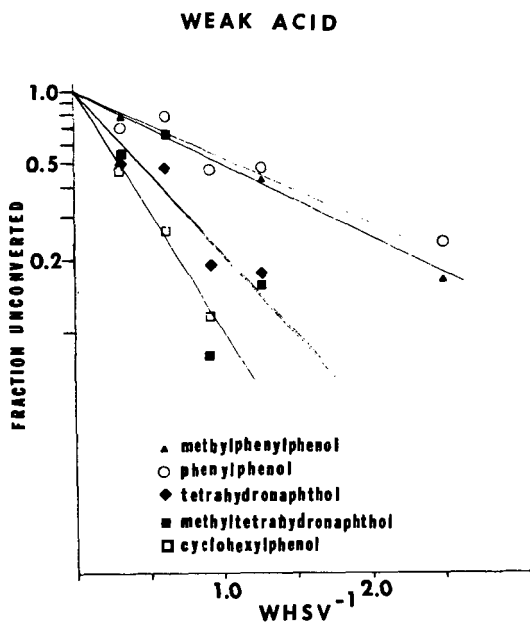


Figure 3

Fraction Unconverted vs. Inverse Space Velocity
Compounds in the Weak Acid

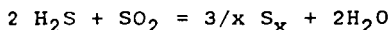
The Kinetics of the Reaction of Hydrogen Sulfide and Sulfur Dioxide in Organic Solvents

Dan W. Neumann and Scott Lynn

Department of Chemical Engineering
University of California
Berkeley, Ca. 94720

I. Introduction

Hydrogen sulfide is an undesirable component found in many industrial process streams. Traditionally its removal and recovery have been accomplished in an absorber-stripper operation, followed by the Claus process in which the H_2S is reacted over alumina catalyst with SO_2 obtained by burning a portion of the inlet stream. The gas-phase reaction to produce sulfur is



This reaction is equilibrium-limited to 95 to 97% conversion in 2 to 4 stages because the temperature must be kept above the dewpoint of sulfur. Additional processing must be provided to reduce the concentration of sulfurous compounds in the effluent to environmentally acceptable levels.

When the reaction between H_2S and SO_2 is carried out in organic liquids at temperatures below $150^{\circ}C$ it is irreversible and goes essentially to completion. In many organic solvents, such as triethylene glycol, dimethyl ether (Triglyme) and diethylene glycol, methyl ether (DGM), the reaction is impractically slow and, at room temperature, the sulfur formed is too finely divided to be readily separated. Urban (3) found that the presence of *N,N*-dimethyl aniline (DMA) increased the crystal size of the precipitated sulfur. Furthermore, DMA accelerates the reaction to the extent that 99+% removal of H_2S is possible with careful selection of the solvent mixture.

The present work was undertaken to study the reaction between H_2S and SO_2 in mixtures of DMA/Triglyme and DMA/DGM. Experiments performed by monitoring the temperature rise of this exothermic reaction in an adiabatic calorimeter show the effects of various solvent compositions on the kinetics of the reaction. Solvent selection criteria for an appropriate process scheme can then be set. This reaction system is suitable for application to a process currently being studied in this laboratory for the removal of hydrogen sulfide from industrial gas streams.

II. Experimental Methods

All rate measurements were made in a 50-ml Erlenmeyer flask that contained a magnetic stir bar and was sealed by a septum cap (see Figure 1). Insulation was provided by a styrofoam block with a hole drilled out for the reactor. Reaction progress was monitored by recording the temperature rise in the form of a millivolt potential produced by a bare, type J thermocouple connected to a chart recorder. A measured quantity of a solution of one reactant was first placed in the reaction vessel. The reaction was initiated when a measured quantity of a solution of

the second reactant at the same temperature was injected quickly into the stirred vessel by syringe.

III. Methods of Analysis

A. Acid-Base Experiments

Reactions between NaOH and HCl were carried out in the calorimeter to determine the rate of mixing, the thermal mass of the apparatus, and the rate of heat loss from the system. The experimental method was that used in the H₂S-SO₂ reactions and the quantities of reactants used gave similar temperature rises. Since the acid-base reaction is practically instantaneous, the time necessary for completion is the mixing time.

A heat balance applied to the apparatus and solution allows calculation of the thermal mass of the reactor. Furthermore, by measuring the decrease in temperature with time after the initial rise, the rate of heat loss from the system can be determined.

A chart recorder trace of thermocouple potential (i.e., temperature) versus time for an acid-base reaction is shown in Fig. 2. The estimated heat leakage from the reaction vessel and styrofoam block corresponds to a rate of temperature loss that is less than 0.002 °C/sec. Thus, there was a loss of about 0.02 °C over the course of a typical H₂S - SO₂ run. Since in the majority of experiments the temperature rise is 5 °C or less, this amounts to an uncertainty of about 0.4% in the maximum temperature.

The average value of t_{mix} is approximately 0.7 sec for the solution volumes of acid and base and stirrer speeds used in these experiments. Presumably, in cases where the reaction between H₂S and SO₂ takes longer than this period, the reaction is then occurring in a homogeneous solution.

From the known heat of reaction for $H^+ + OH^- (= -13.4$ kcal/mole of H₂O formed) and the heat capacity of the aqueous solutions (approximated as water, $C_p = 1$ Cal/g °C), the thermal mass of the apparatus was determined to be 0.6 cal/°C. Since in these experiments the thermal mass of the solution for a typical run was 12-15 cal/°C., the contribution of the apparatus to the total heat capacity of the system was small.

B. Kinetics

If the reaction between H₂S and SO₂ is first order in both reactants, then the differential rate equation for the disappearance of SO₂ or H₂S is

$$-dC_A/dt = -1/2 dC_B/dt = k_2 C_A C_B \quad 1)$$

By stoichiometry

$$C_B = C_B^0 - 2(C_A^0 - C_A) \quad 2)$$

in which the superscript 0 refers to time = 0. Substituting Eq. 2 into Eq. 1 and rearranging yields the following rate expression:

$$k_2 dt = dC_A / (C_A * (2C_A - 2C_A^0 + C_B^0)) \quad 3)$$

Integration of Eq. 3 and simplification gives

$$k_2 t = (1/(2C_A^0 - C_B^0)) \ln ((C_B^0/C_A^0) * (C_A/C_B)) \quad 4)$$

If a reaction is first order with respect to both A and B then a plot of the integrated rate expression on the right-hand side of Eq. 4 versus time should lie on a straight line with a slope of k_2 . Note that when the initial concentrations of H_2S and SO_2 are stoichiometrically equivalent, Eq. 4 reduces to the more familiar second-order relationship

$$k_2 t = 1/C_A^2 - 1/C_A^{02} \quad 5)$$

Equation 4 is in the form of concentration and time whereas the quantities measured experimentally are temperature and time. If the temperature rise for the exothermic reaction between H_2S and SO_2 is assumed to be proportional to the extent of reaction (i.e. is a measure of reaction progress) and if the maximum temperature corresponds to complete reaction (fraction conversion = 1.0) with any uncertainty arising from thermal losses, then for any time $t < t_{max}$ the concentration of the limiting component is related to the temperature rise by the expression

$$C = C^0 * (1 - \Delta T/\Delta T_m) \quad 6)$$

From this concentration and the known stoichiometry, the concentration of the other reactant can be calculated. In order to keep the uncertainty arising from thermal losses to a minimum, only temperature rises less than 90% of the maximum value are used for determining reaction-rate constants.

In the preceding analysis perfect mixing has been assumed. Since these experiments require the injection of one of the reactant solutions into the other, a finite period, whose length depends on the sample volumes, solvent viscosity, and stirrer speed, is needed to completely mix the components. Before mixing is complete, local inhomogeneities exist in which one of the reactants is in large excess. The other reactant is rapidly depleted, effectively reducing the reaction rate in these regions to zero. Overall, the experimentally measured rate is lowered and the kinetics of the reaction under such conditions is of uncertain significance. Once the solutions are thoroughly mixed, the rate becomes that for the homogeneous reaction. The rate constant can be determined from plots of the integrated rate expression (Eq. 4) versus time by considering only the portion of the plot for which the time is greater than the mixing time.

C. Heat of Reaction

The heat of reaction for each of the experiments is calculated from the measured temperature rise and the thermal properties of the system. An enthalpy balance yields

$$\Delta H_{rxn} = ((mC_p)_s + (mC_p)_{app}\Delta T)/1000 n_L \quad 7)$$

The heat capacity of the organic solution, which was assumed to include all solvents and products, was estimated by a group contribution method applied to the bulk solvent used in a given run. Calculations for Triglyme and DGM using Missenard's group contribution method (2) give a value of $C_p \sim 0.5 \text{ cal/g-}^\circ\text{C}$.

IV. Results and Discussion

A. Results for the Reaction of H_2S and SO_2 in Triglyme/DMA/ H_2O

Kinetic data were analyzed using equation Eq. 4. Plots of the concentration expression on the right side of Eq. 4 versus time yield a straight line (in the region $t > t_{\text{mix}}$) with a slope of value k_2 when the reaction follows second-order kinetics. Data pairs of potential/time obtained from the chart-recorder traces were converted into concentration/time pairs and plotted in the integrated rate form.

A sample plot for the reaction of H_2S and SO_2 in a DMA/Triglyme mixture is shown in Fig. 3. Values of k_2 were obtained from similar plots by drawing the best straight line through the data. The curvature at times less than 1 sec. results from the finite time required for injecting the SO_2 sample and mixing the solution. In nearly all of the runs the time intercept, as found by extrapolating the line drawn through the integrated rate data back to the time axis, is about 0.5 to 0.8 seconds. These values, which approximate the mixing time in the HCl - NaOH experiments, show little variation from run to run and thereby indicate a high degree of reproducibility in the experimental conditions and technique. Furthermore, since this result agrees with the mixing time obtained in the acid-base experiments, data points at longer times presumably represent the progress of the reaction in a well-mixed solution.

Most of the experiments presented here were performed with nearly stoichiometric equivalents of H_2S and SO_2 . Additional experiments were carried out with the ratio of H_2S to SO_2 varying from about 2:1 to 1:2. In all cases the second-order rate expression provided the best straight line fit to the data in spite of a four-fold change in SO_2 concentration. Attempts to analyze the data using a rate expression which is second order in H_2S and first order in SO_2 yielded non-linear integrated rate plots.

The results for the reaction in Triglyme with DMA and water present are summarized in Fig. 4, where the second-order rate constant is plotted as a function of wt% DMA for various H_2O concentrations. With pure Triglyme as the sole solvent, plots of the integrated rate expression versus time are non-linear, increasing in slope as time progresses. Tangents to these curves correspond to k_2 values of 0.5 lit/mole-s or lower. The curvature, which reflects an increase of the rate constant with time, may be due to an autocatalytic effect of water formed during the reaction or possibly to a change in the reaction mechanism. Note that while a mixture of water/Triglyme speeds the reaction, it is unclear whether the same reaction pathway is followed since some of the integrated rate plots are non-linear. Perhaps other products such as sulfoxy acids, which frequently form in aqueous media, are being created in these cases.

When DMA is added to Triglyme, the integrated rate plots become linear, i.e. there is a first - order dependence on both H_2S and SO_2 . Furthermore, there is a substantial increase in the rate when DMA is added to the Triglyme. Addition of only 2 wt% DMA more than doubles the reaction rate over that observed for Triglyme alone. Increasing the DMA concentration increases the rate constant, k_2 , which asymptotically approaches a value of 8 lit/mole-s.

The presence of water in DMA/Triglyme greatly accelerates the rate as evidenced in Fig.4. Addition of 4 to 5 wt% H₂O doubles the observed rate constant. Also, the value of k_2 for the mixed solvents exceeds the sum of those for the reaction carried out with only one of the catalysts (DMA or H₂O) present. This suggests a synergism between the effects of the water and DMA.

B. Results for the Reaction in DMA/DGM/Water

The kinetic behavior of the reaction in DGM alone is similar to that observed for Triglyme. DGM has little or no catalytic effect, and plots of the integrated rate expression exhibit an increase in rate with time. However, values for k_2 are considerably higher when a given wt% DMA is added to DGM than are those found in the Triglyme runs. The rate constants for the reaction of H₂S and SO₂ in DMA/DGM mixtures are shown in Fig. 5. The DGM also seems to have a catalytic effect on the reaction; increasing the DMA percentage toward pure DMA causes a noticeable decrease in rate as opposed to the monotonic increase observed in Triglyme mixtures. The maximum value of k_2 , which is approximately 20 lit/mole-s, is more than twice as large as that obtained in the Triglyme/DMA cases with no water present.

The addition of water to DMA/DGM mixtures has little or no effect on the rate, as is reflected in the data presented in Table 1. At 10 wt% DMA the rate constant has attained its maximum value and the addition of water does not increase the rate.

A few runs with 2.5 wt% DMA in DGM, performed at 7 to 10 °C, yielded an average k_2 of 4.5 lit/mole-s (see Table 2). On the basis of these data and those in Fig. 5, the estimated activation energy is 7.4 kcal/mole, which corresponds to a doubling of the rate every 20 °C.

C. Results for the Reaction in DMA/Triglyme/Methanol

A reasonable hypothesis to explain the fact that both H₂O and DGM accelerate the reaction between H₂S and SO₂ in the presence of DMA is that the hydroxyl group is exerting a positive catalytic effect. In order to further substantiate this idea, a few experiments were performed in which methanol was added to DMA/Triglyme. The data are summarized in Table 3. The presence of the indicated methanol concentration increased the rate constant by a factor of 6 over that for the same concentration of DMA alone in Triglyme. As in the DMA/Triglyme/Water runs, adding methanol to the mixture enhances the observed reaction rate. Also, the rate constant for this mixture, which contains an eight-to-one mole ratio of methanol to DMA, is about the same as the value of k_2 for the same molar ratio of DGM to DMA. Thus, for cases in which the same ratio of hydroxyl groups to DMA is used, similar effects on the reaction kinetics might be expected.

D. Heat of Reaction

The heat of reaction between H₂S and SO₂, taken as the average for a large number of data points, is 28 to 29 kcal/mole of SO₂ reacted. This value seems to apply equally well to all mixtures of the solvents used in these experiments. Evidently, effects such as heats of solution are small or similar in magnitude for the range of cases considered.

E. Summary

From these experimental results it is readily apparent that the presence of DMA greatly accelerates the reaction of H_2S and SO_2 in organic solvents. The nitrogen of the amine, which is noted for its ability to form complexes with sulfur dioxide (1), presumably provides a favorable site at which the reaction can occur. This effect seems to be dependent on the concentration of the catalytic agent rather than its ratio to either of the reacting components, since the mole ratio of DMA to SO_2 exceeds one at less than 1 wt% DMA in most of the experiments. This suggests that the enhancement is related to the accessibility of sites rather than the actual number present. In the DMA/Triglyme experiments the rate constant increases with increasing DMA, implying that the Triglyme has little or no catalytic effect and actually reduces the rate by diluting the concentration of useful reaction sites.

For the reaction in DGM an additional factor is found to be important. The DGM appears to work with DMA in accelerating the reaction, producing a maximum rate when intermediate concentrations of both solvents are present. This enhancement seems to be related to a catalytic effect of the OH group of the DGM that is synergistic with DMA. Further evidence of the OH effect can be seen in the results for the reaction in DMA/Triglyme with water present; indeed this effect may be expected for alcohols in general since the experiments performed with DMA/ Triglyme/Methanol yielded similar results. Determination of whether the hydroxyl provides an alternate reaction site or speeds an intermediate or parallel step or causes some other enhancement will require further investigation. It is clear however, that mixtures of DMA with glycol mono ethers are good solvents for the catalysis of the reaction between H_2S and SO_2 to form sulfur.

Acknowledgement

This work was supported by the Morgantown Energy Technology Center, Assistant Secretary for Fossil Energy, Office of Coal Utilization, Advanced Research and Technology Development, Division of Surface Coal Gasification, through the US Department of Energy under Contract No. DE-AC03-76SF00098.

References

1. Hill, Arthur E., and Thomas B. Fitzgerald, "The Compounds of Sulfur Dioxide with Various Amines," J. of Am. Chem. Soc., 57, 250 (1935).
2. Reid, Robert C. , John M. Prausnitz, and Thomas K. Sherwood, "The Properties of Gases and Liquids", McGraw-Hill, NY, (1977).
3. Urban, Peter, "Production of Sulfur," U.S. Patent #2,987,379 (June 1961).

Notation

- C_A, C_B = Concentration of SO_2 and H_2S at time t (mole/lit)
 C_A^0, C_B^0 = Concentration of SO_2 and H_2S at time 0 (mole/lit)
 ΔH_{rxn} = Heat of reaction (kcal/mole)
 k_2 = Second-Order Rate Constant (lit/mole-s)
 $(mC_p)_s$ = Thermal mass of solution (cal/°C)
 $(mC_p)_{app}$ = Thermal mass of apparatus (cal/°C)
 n_L = Moles of limiting reactant
 t = time (sec)
 $\Delta T, \Delta T_m$ = Temp. change and maximum temp. change (°C)

Table 1
Rate Constants for the Reaction of H_2S and SO_2 in
DMA/DGM with Water Added

Wt% H_2O	Wt% DMA	k_2 (lit/mole-s)
0.5	9.8	20.4
0.5	9.8	21.6
1.4	9.7	22.8
1.6	9.7	22.1
2.4	9.6	21.3
2.6	9.6	23.5

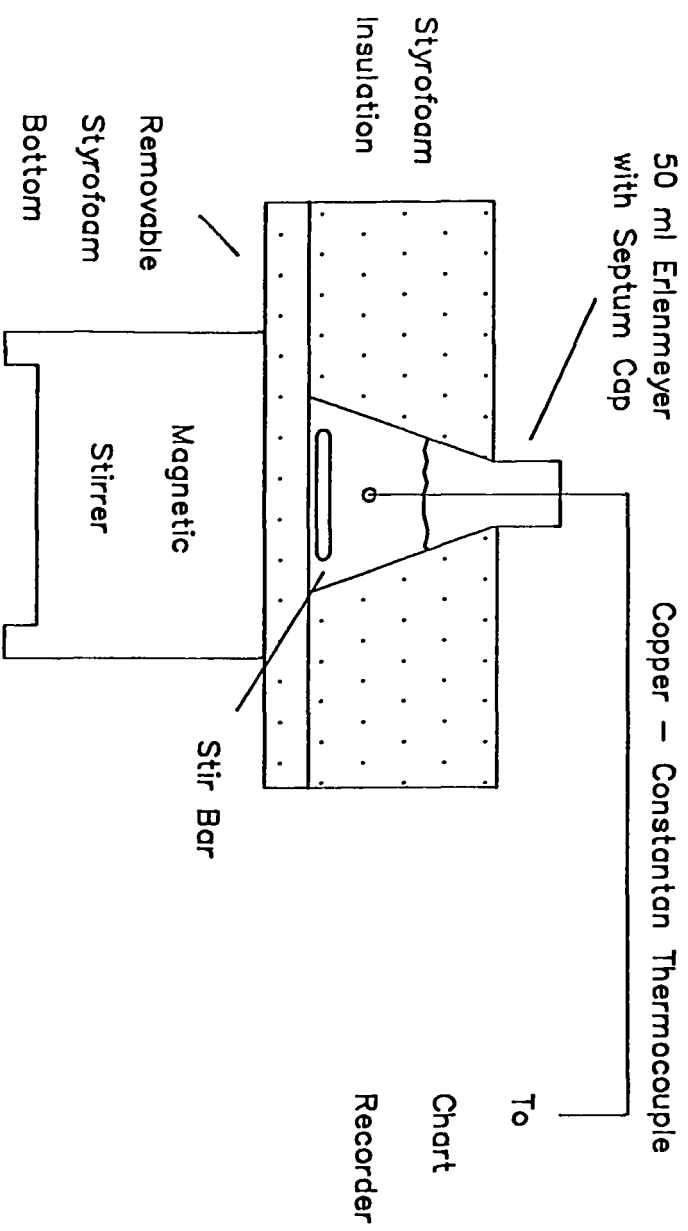
Table 2
Rate Constants for the Reaction Between H_2S and SO_2 in
2.5 Wt% DMA in DGM at 7-10 °C

RUN	k_2 (lit/mole-s)
1	2.5
2	4.3
3	5.0
4	4.3

Table 3
Rate Constants for the Reaction of H_2S and SO_2 in
DMA/Triglyme/Methanol Mixtures

RUN	Wt% DMA	WT% Methanol	k_2 (lit/mole-s)
1	10.1	45.1	23.5
2	10.1	45.2	24.0
3	10.1	45.1	22.8

Figure 1
Experimental Apparatus



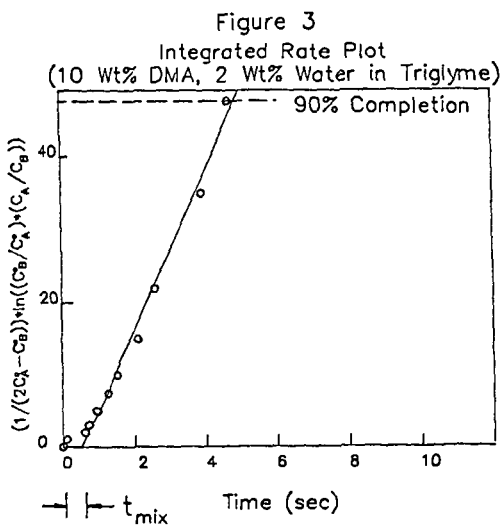
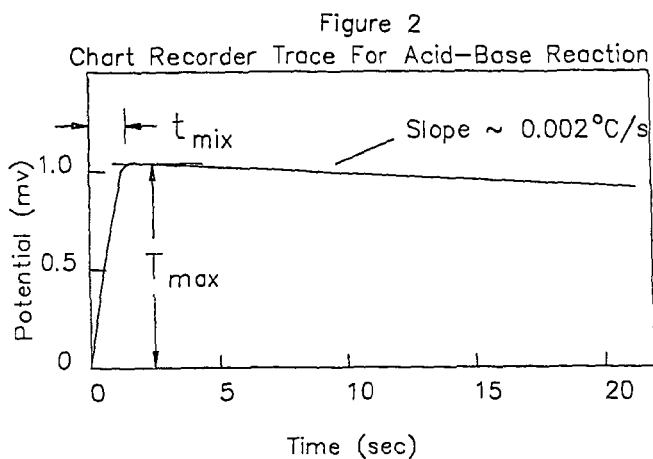


Figure 4

Variation of Second-Order Rate Constant
with DMA and Water Content for the Reaction
of Hydrogen Sulfide and Sulfur Dioxide in Triglyme

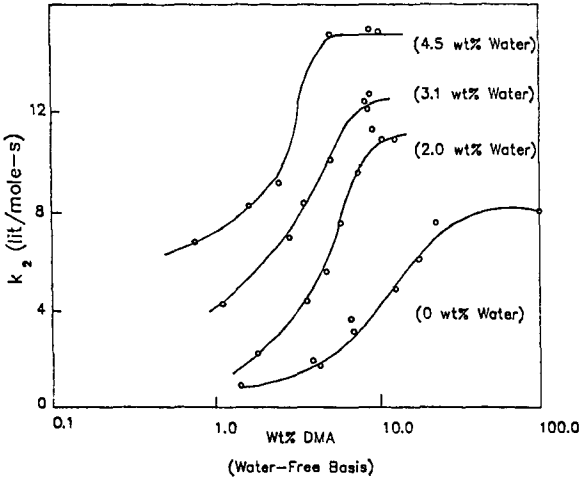
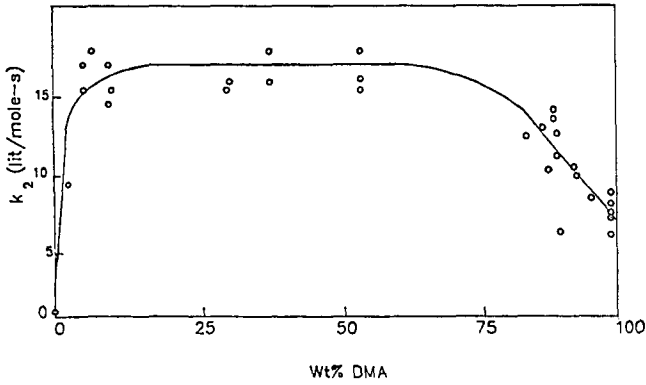


Figure 5

Variation of Second-Order Rate Constant with Wt% DMA
For DMA in DGM at 17-23°C (No Water)



PRODUCTION OF HYDROGEN FROM LOW HEATING VALUE FUEL GASES BY THE BEACON PROCESS

J. Blumenthal, T. Fitzgerald, A. Grossman, E. Koutsoukos, B. Pote

TRW, One Space Park, Redondo Beach, California 90278

M. Gbate

Department of Energy, METC, P.O.. Box 880, Collins Ferry Road

Morgantown, West Virginia 26505

Background

BEACON is an acronym for Btu Extraction And CONcentration. The process is based on the catalytic deposition of a highly reactive carbon (C*) from low heating value gases (LBG = low Btu gas). As illustrated in Figure 1 the BEACON process involves circulating a very easily fluidizable, solid carbonaceous material containing a catalyst between two fluid bed reactors.

In one reactor the solid material contacts the low heating value fuel gas feedstock resulting in the rapid deposition of very reactive carbonaceous material by reactions of the type:



Thus, in this reactor the incoming carbonaceous material and catalyst are enriched in carbon content through the deposition process and the low heating value fuel gas is depleted in energy content by an amount which is nearly equal to the heating value of the deposited carbon. The fuel gas is brought into the fluid bed carbon deposition reactor at near ambient temperature and the depleted fuel gas exits the reactor at 450°C to 550°C. Thus, most of the exothermic heat associated with carbon deposition is taken up in the depleted fuel gas as sensible heat in the nitrogen diluent, available for steam or power generation.

The carbon rich, solid, carbonaceous material and associated catalyst produced in the deposition reactor is separated from depleted fuel gas and circulated to a second reactor where the material is contacted with steam. In this reactor the steam-carbon reaction is very rapid at temperatures as low as 550°C or some 300°C below the temperature at which coals or chars will react effectively with steam. Depending on operating conditions (pressure, temperature and steam utilization) and catalyst type, either of the following overall reactions may predominate:



or



Heat must be supplied for the steam-carbon reactions described above. However, since the reaction temperature is modest (550-650°C) this heat can readily be supplied (indirectly) from the hot, depleted, and fully combusted fuel gas. Thus, a part of the residual energy content of the depleted fuel gas is used to drive the

steam-carbon reactions. This endothermic heat of reaction, of course, adds to the final total heating value of product methane or hydrogen at near 100% efficiency. That is to say, the higher heating value of the product methane or hydrogen rich gas exceeds the heating value of the reactant carbon by an amount equal to the endothermic heat of reaction.

To complete the solids circulation loop, carbon lean solids from the steaming reactor are returned to the carbon deposition reactor for carbon enrichment. For example, the carbon lean solids may contain 50-60% carbon and the carbon rich solids may contain 80-90% carbon.

In the BEACON technology there are three key areas of technical advantage:

1. A novel chemistry which results in very fast reactions at moderate temperature.
2. An ability through modifications of operating conditions and catalysts to produce either methane or hydrogen as a primary product.
3. An intermediate carbonaceous material and associated catalyst which has excellent fluid mechanical properties.

In both the carbon deposition and steaming reactions, utilizing the catalysts developed, near equilibrium compositions are obtained with gas-solid contact times that are well within commercially practical ranges. Carbon deposition is rapid above 400°C and the steam-carbon reaction becomes effective above 550°C.

The fluid mechanical properties of unsupported carbonaceous material are very different from other solid powders. Of great importance is the fact that this material fluidizes very well at commercially reasonable gas velocities.

Experimental Approach and Theoretical Comparisons

The objective of the work described in this paper was to demonstrate the viability of a catalyst system which is selective for hydrogen production in the reaction of deposited carbon with steam. In this case we want to suppress the formation of methane as completely as possible in the steaming reaction. In assessing our results we will compare the experimental measurements with two types of equilibrium calculations. The first type of thermochemical calculation allows methane and all other possible species to be present in the equilibrium product mixture. The second calculation excludes all hydrocarbon species (principally CH₄) from the calculation and gives a pseudo-equilibrium distribution of product species under conditions where methane is not allowed to form.

The experimental system shown in Figure 2 and described previously (Ref. 1) was used in the investigation. The system is a two reactor apparatus based on a variable differential pressure transfer line concept for the transfer of solids between BEACON carbon deposition and carbon gasification reactors. The "huff-puff" transfer system does not require gas/solids separation prior to transfer, and therefore it is simpler than a lock-hopper type system for fluidized bed operations. Adaptation of the "huff-puff" concept in BEACON processing was considered possible because of the unique properties of the solids-gas mixtures which give rise to stable fluid beds.

In this tandem concept the two reactors are connected with a fluid bed transfer line located below the top of the beds. Transfer is accomplished by establishing a small differential pressure between the two reactors and opening the transfer line valve. Solids are transferred back and forth by changing the sign of the differential pressure. About 10% of the bed is transferred each time. The

two reactors can be operated at different operating conditions, except pressure, as needed to optimize deposition or gasification; pressure, however, must be nearly equal in the reactors. Two additional requirements are that the relative size of the two reactors be such that the quantities of carbon deposited and gasified per unit time are equal and that both reactors operate under fluidized bed conditions. Ranges of allowable operating conditions were as follows:

<u>Parameter</u>	<u>Deposition Reactor</u>	<u>Steaming Reactor</u>
Temperature	400-600°C	500-750°C
Pressure	1-10 Atm	1-10 Atm
Gas Velocity	5-45 cm/sec	5-56 cm/sec
Feed Gas Composition:		
o Nitrogen	10-85%	0-50%
o Hydrogen	5-30%	0
o Carbon Monoxide	10-50%	0
o Carbon Dioxide	0-10%	0
o Steam	0	50-100%

The system shown in Figure 2 consists of the following sections: gas feed system, steam boiler, carbon deposition reactor, steam gasification reactor, product gas cleanup train, reactor pressure control and product gas metering system, solids transfer system, and data acquisition system. The deposition reactor has a 6-inch inside diameter and the gasifier a 3-inch inside diameter (the difference in reactor size was dictated by the difference in deposition and gasification rates at the desired operating ranges). Both reactors are constructed from 316 stainless steel parts and are surface aluminized by the Alon Process to prevent catalyst contamination from the reactor walls (especially through carburization of the deposition reactor walls).

Carbon deposition and steaming took place simultaneously and at equal rates. Typical rates were approximately 400 grams carbon deposited or steamed per hour; thus, the net solids transfer from the deposition reactor to the gasifier was about 400 grams per hour. Nominally, transfers were conducted about once an hour; approximately 700 grams were transferred from the carburizer to the gasifier and about 300 grams in the opposite direction. These quantities represented about 10% of the total solids in the system so that the disturbance of steady state was minor (the transfer was noticeable for one gas chromatogram of the product gas of the gasifier but had no effect on the product gas of the carburizer). Solids were transferred from the bottom of the reaction zone of one reactor to the top of the reaction zone of the other reactor; occasionally, the direction was reversed. The two-directional transfer operation took about three minutes, including the time (about one minute) required for system equilibration between the single transfers.

A single batch of catalyst solids (No. 11) which had shown outstanding activity and selectivity (methane suppression) in previous, small atmospheric pressure laboratory tests was subjected to approximately 375 hours of processing (simultaneous carbon deposition and steaming in separate reactors). Processing time consisted of 265 hours of steady state operation and about 110 hours of transient operation (mostly start-up and shutdown). Steady state processing time consisted of about 200 hours of operation at 4.4 atmospheres (50 psig), 50 hours at 6.1 atmospheres (75 psig), and 15 hours at 7.8 atmospheres (100 psig) reactor pressure.

The nominal conditions during the multi-cycle testing of Catalyst No. 11 solids were 620°C and six centimeters per second linear superficial velocity for steam gasification and 400°C and 15 centimeters per second velocity for carbon deposition at the above three pressures. The feed to the gasifier was 100% steam, but in the reaction zone it was diluted by approximately 20% v/v nitrogen gas used to maintain the DP legs and solids transfer lines free of solids (purge gas). The nominal deposition reactor feed gas composition was 10% v/v CO, 5% v/v H₂, with the balance being nitrogen gas.

Results

Figure 3 summarizes the catalyst performance data generated during the 375 hours of simultaneous operation (265 hours of steady state processing). The top portion of Figure 3 summarizes the performance of the carbon deposition operation expressed in terms of "fuel" (CO and H₂) utilization. Carbon monoxide utilization was near equilibrium and constant. Hydrogen utilization was high and also constant throughout the 265 hours of steady state processing. The middle and bottom graph of Figure 3 summarize the data pertaining to the performance of the steam gasification operation. Over the range of pressures investigated, nominally 80% methane suppression was obtained at equilibrium steam utilization for the duration of the 265 hours of steady state operation. Neither the deposition nor the gasification data revealed any trend of catalyst deterioration.

The stability of Catalyst No. 11 performance is also evident from the data presented in Tables 1 and 2, where a set of product gas composition data (dry and nitrogen free) is presented for every 50 hours of steady state operation. Table 1 summarizes steaming data which are compared to compositions predicted by thermodynamics for equilibrium operation at 650°C, 4.4 and 6.1 atmospheres (50 and 75 psig). The comparison of experimental data to equilibrium composition reveals that after 50 hours of processing time some CO (and steam) have shifted to CO₂ and H₂. It is expected that this shift occurs in the transition and expansion zone of the reactor. This conclusion is consistent with on-line DP monitoring which indicated an increase in the mass of solids contained in the expansion zone during the latter part of testing. Table 2 presents data for the carbon deposition operation. Product gas composition stability is excellent, CO conversion is high and approaches equilibrium values, but hydrogen conversion is significantly lower than equilibrium predicted values.

Including laboratory data, four pressures were investigated during the course of performance testing of Catalyst No. 11. Figure 4 illustrates the effect of reactor pressure on steam utilization and methane concentration in the product gas during steam gasification of Catalyst No. 11 solids at 620°C. The experimental data are compared to thermodynamically predicted values for the same conditions (solid lines on Figure 4). Methane suppression was nominally 80% or greater at all pressures investigated. The experimental values of the steam utilization fall in between the thermodynamically predicted values represented by the solid lines for normal and zero methane equilibria. This was expected since methane suppression was not complete.

Acknowledgment

This work was performed by TRW under Department of Energy Cooperative Agreement DE-FC21-80MC14400.

Reference

1. Blumenthal, J. L., et al, "Tandem Reactor Testing of the BEACON System," 11th Energy Technology Conference, March 20, 1984, Washington, D.C.

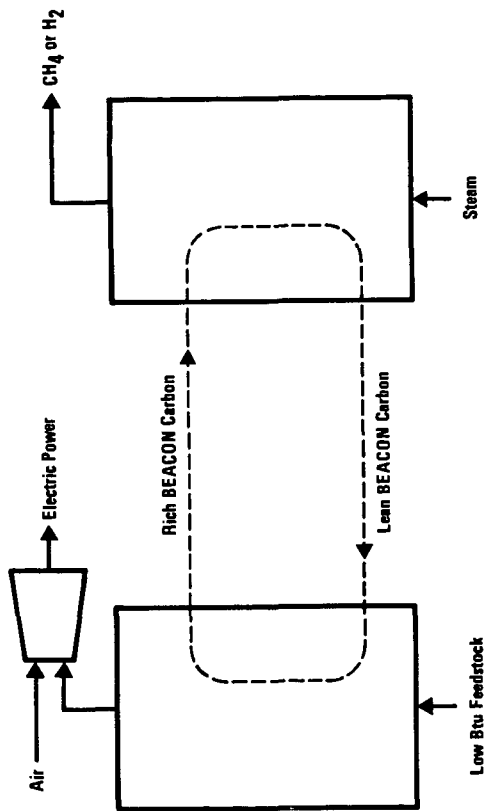


FIGURE 1. BEACON PROCESS CONFIGURATION

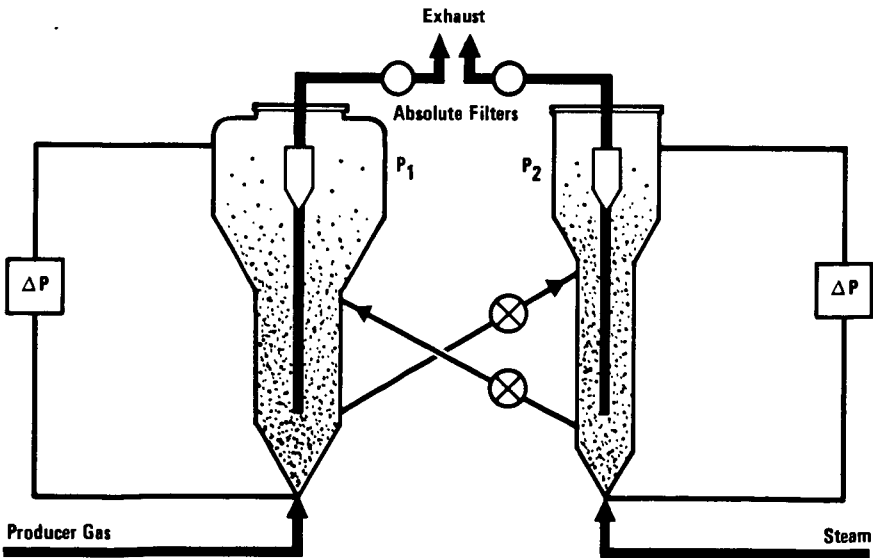
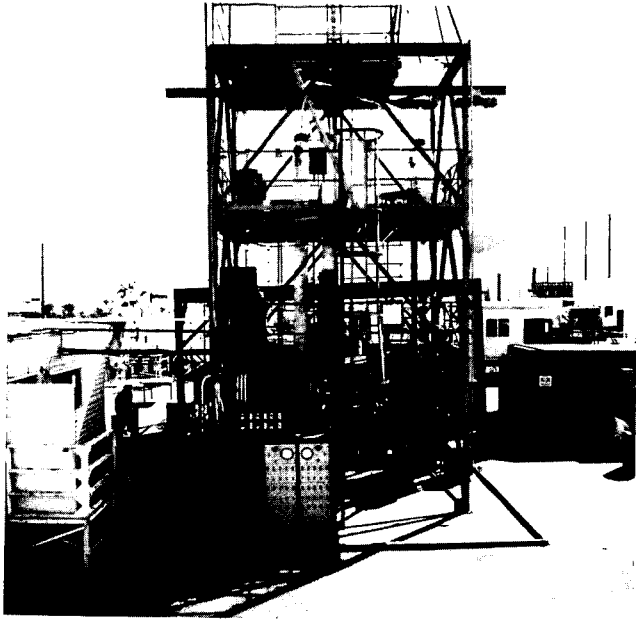
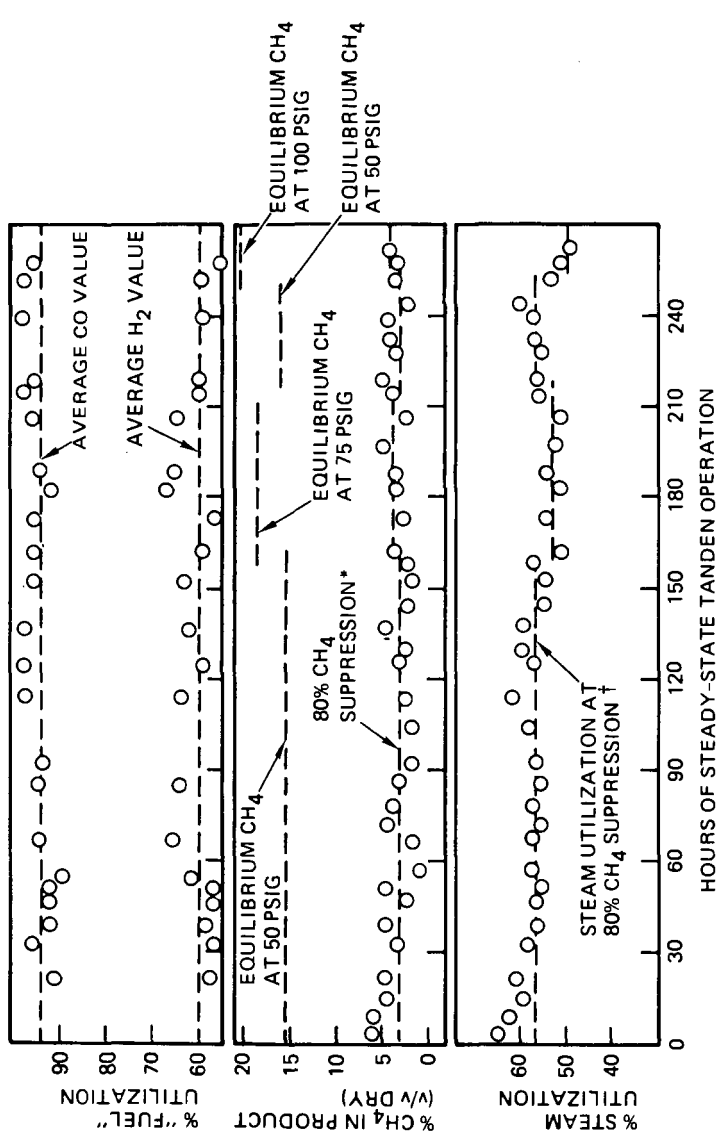


FIGURE 2. EXPERIMENTAL APPARATUS



*EQUILIBRIUM CH₄ AT 50/75/100 PSIG IS 15.8/18.3/20.2 PERCENT. AT 80% SUPPRESSION, METHANE IS 3.2/3.7/4.0 PERCENT RESPECTIVELY.

†EQUILIBRIUM STEAM UTILIZATION AT : 50/75/100 PSIG IS 64.7/63.0/61.8 PERCENT AT NORMAL METHANE (METHANE IS ALLOWED TO FORM) AND 54.2/50.5/47.7 PERCENT AT 100% CH₄ SUPPRESSION (METHANE IS NOT PERMITTED TO FORM). BY INTERPOLATION, AT 80% CH₄ SUPPRESSION, STEAM UTILIZATION SHOULD BE 56.3/33.0/50.5 PERCENT, RESPECTIVELY.

FIGURE 3. STABILITY TESTING OF CATALYST NO. 11 IN TANDEM REACTORS (400°C/620°C, 50/75/100 PSIG)

TABLE 1. STABILITY OF PRODUCT GAS COMPOSITION IN TANDEM REACTORS (STEAM GASIFICATION OF CATALYST NO. 11 SOLIDS AT 620°C, 50 PSIG AND 75 PSIG)

Species	Thermodynamically Predicted Composition				Product Composition, 5 v/v Versus Hours of Operation					
	50 Psig		75 Psig		50 Hrs*	100 Hrs*	150 Hrs*	200 Hrs**	250 Hrs*	
	Normal	Zero Methane	Normal	Zero Methane						
CH ₄	15.8	0	18.3	0	4	3	2	3	2	
H ₂	41.2	62.5	38.4	62.9	57	61	60	63	62	
CO	13.0	12.3	11.5	11.0	12	9	7	6	7	
CO ₂	30.0	25.2	31.8	26.1	27	27	31	28	29	
% Steam Utilization	64.7	54.2	63.0	50.5	55	60	54	54	58	
% Methane Suppression	0	100	0	100	75	81	87	84	87	

● Typical Feed Composition: 80% v/v Steam, 20% v/v N₂ (Nitrogen was used to purge DP probes)

* 50 psig data

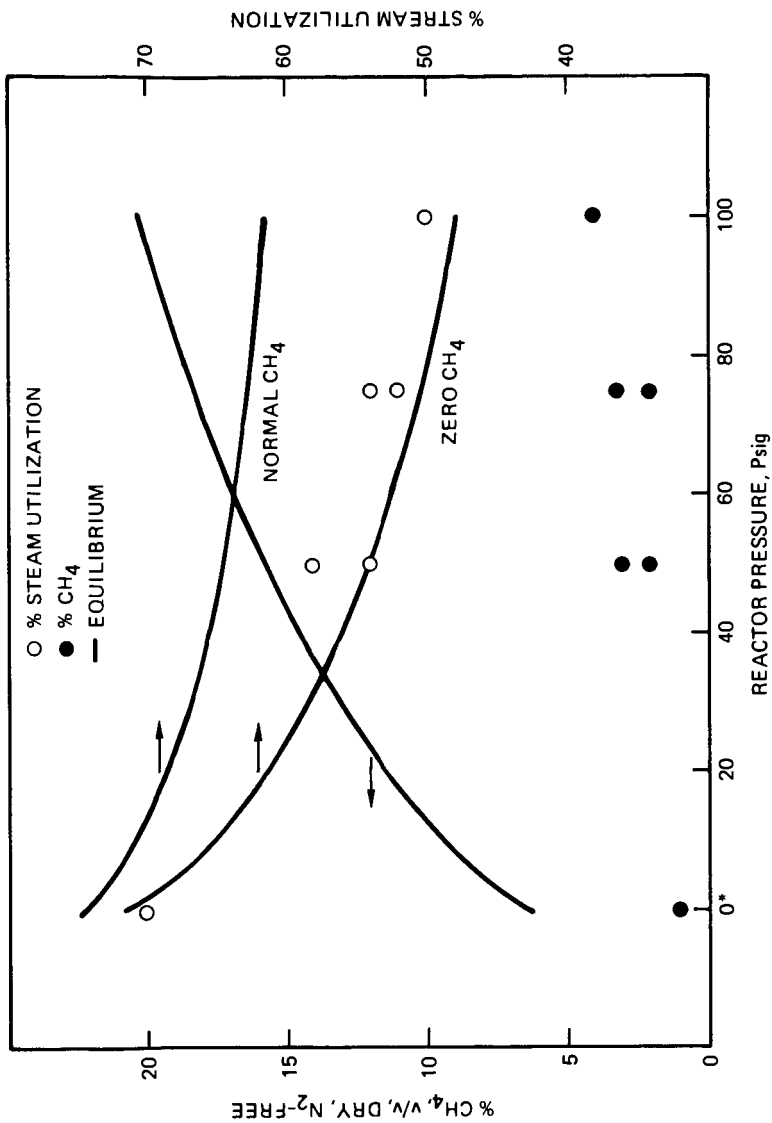
** 75 psig data

TABLE 2. STABILITY OF PRODUCT GAS COMPOSITION IN TANDEM REACTORS (CARBON DEPOSITION ON CATALYST NO. 11 SOLIDS AT 400°C, 50 PSIG AND 75 PSIG)

Specie	Thermodynamically Predicted Composition			Hours of Operation (Test Data)					
	50 Psig	50 Psig	75 Psig	50 Hrs*	100 Hrs*	150 Hrs*	200 Hrs**	250 Hrs*	
A. Feed Gas Composition, % v/v (Balance Nitrogen)									
CO	9	13	13	9	13	11	13	11	
H ₂	4	6	6	4	6	5	6	4	
B. Product Gas Composition, % v/v (Nitrogen Free)									
CH ₄	8.5	10.0	10.6	2	4	4	6	4	
H ₂	16.1	14.5	12.9	28	25	26	29	25	
CO	1.6	1.4	1.2	12	4	6	4	5	
CO ₂	73.8	74.1	75.3	58	67	64	61	66	
C. Fuel Utilization									
% CO	99.2	99.4	99.5	92	97	96	97	97	
% H ₂	82.6	85.3	87.3	56	63	61	59	58	

* 50 psig data

** 75 psig data



*AMBIENT PRESSURE DATA GENERATED AT 100% STEAM FEED. EQUILIBRIUM CURVES AND PRESSURIZED DATA ARE FOR A 80% v/v STEAM, 20% v/v N₂ REACTOR FEED.

FIGURE 4. EFFECT OF PRESSURE ON PERFORMANCE OF CATALYST NO. 11 IN HYDROGEN PRODUCTION FROM BEACON CARBON (620 °C)